

A renormalization group analysis of the one-dimensional extended Hubbard model

M. Ménard¹ and C. Bourbonnais^{1,2}

¹ *Regroupement Québécois sur les Matériaux de Pointe, Département de physique,
Université de Sherbrooke, Sherbrooke, Québec, Canada, J1K-2R1 and*

² *Canadian Institute for Advanced Research, Toronto, Canada*

(Dated: September 22, 2010)

The phase diagram of the one-dimensional extended Hubbard model at half-filling is investigated by a weak coupling renormalization group method applicable beyond the usual continuum limit for the electron spectrum and coupling constants. We analyze the influence of irrelevant momentum dependent interactions on asymptotic properties of the correlation functions and the nature of dominant phases for the lattice model under study.

PACS numbers:

I. INTRODUCTION

The application of the renormalization group (RG) and boson representation methods to one-dimensional (1D) models of interacting electrons have provided over the last four decades considerable insight into the nature of correlations in low dimensional systems¹⁻⁴. This has been largely achieved by treating the models in the continuum field-theory limit, corresponding to the so-called weak coupling 1D electron gas (EG) model. There are notable exceptions, however, where the 1D-EG model clearly fails to reveal the nature of correlations at long distance. These situations are likely to occur in models for which lattice effects, albeit related to irrelevant terms in the RG sense, do affect the asymptotic behavior of electronic correlations and then the nature of the ground state.

A well documented case is encountered in the extended Hubbard model at half-filling, which is defined on a lattice in terms of intersite hopping and the on-site and nearest-neighbor sites couplings U and V . On numerical side, exact diagonalization^{5,6}, quantum Monte Carlo⁷ and density-matrix renormalization group analysis⁸ have established the incursion of a bond order-wave (BOW) state over a finite region of the phase diagram surrounding the line $U = 2V > 0$, a result at variance with the spin density-wave (SDW) to charge density-wave (CDW) transition found in the theory of the 1D EG^{1,9,10}.

Using perturbation theory arguments, Tsuchiizu and Furasaki¹¹ showed how high-energy or short-distance degrees of freedom can modify the initial conditions of an effective low energy continuum theory and favor the occurrence of a BOW phase that enfolds the $U = 2V > 0$ line in weak coupling. The influence of the lattice on the nature of the ordered phase in this region of the phase diagram has been investigated by Tam *et al.*,¹² using the functional RG method. The scaling transformation of interactions, which in this framework gather both their marginal and momentum dependent parts, was obtained for a tight-binding electron spectrum in a finite momentum space. The CDW/SDW degeneracy that takes place at $U = 2V$ in the continuum limit, is thus lifted and a BOW state stabilized over a portion of the phase dia-

gram that grows in size with increasing U , consistently with numerical calculations at weak coupling. The functional RG method, however, tells us not as much about the structure of leading irrelevant terms and how these modify scaling and the nature of ordered states of the continuum theory.

In this work we address this issue from a different perspective that generalizes the weak coupling momentum shell Kadanoff-Wilson (K-W) RG method to lattice models^{13,14}. The proposed approach exceeds the limitations of the continuum approximation and takes into account the tight-binding structure of the spectrum and its impact on the scaling transformation of both local and momentum dependent interactions of the extended Hubbard model¹⁵. The latter couplings, though irrelevant, are found to affect the flow of the former interactions. A modification of certain portions of the phase diagram follows; in particular, the BOW phase is found to insert in a finite region near the $U = 2V > 0$ line, in agreement with the results of numerical calculations.

In Sec. II, we introduce the model and set out the basic steps of the momentum shell RG transformation for the partition function. In Sec. III, the RG flow equations for the coupling constants and the most singular response functions are analyzed at the one-loop level and different U and V . The phase diagram is mapped out in weak coupling. We conclude in Sec. IV.

II. THE EXTENDED HUBBARD MODEL AND THE RENORMALIZATION GROUP FORMULATION

A. The model

We consider the extended Hubbard Hamiltonian for a one-dimensional lattice,

$$H = -t \sum_{i,\sigma} (c_{i+1,\sigma}^\dagger c_{i,\sigma} + c_{i,\sigma}^\dagger c_{i+1,\sigma}) + U \sum_i n_{i,\uparrow} n_{i,\downarrow} + V \sum_i n_i n_{i+1}, \quad (1)$$

where t is the hopping integral, $n_{i,\sigma} = c_{i,\sigma}^\dagger c_{i,\sigma}$ is the occupation number on site i for the spin orientation $\sigma = \uparrow$

, \downarrow , and $n_i = n_{i,\uparrow} + n_{i,\downarrow}$. In Fourier space the Hamiltonian can be written in the form

$$\begin{aligned}
H = & \sum_{p,k,\sigma} \epsilon_k c_{p,k,\sigma}^\dagger c_{p,k,\sigma} + \frac{1}{L} \sum_{\{k,q,\sigma\}} \left(g_1 + 2\bar{g}_1 \sin^2 \frac{q}{2} \right) c_{+,k_1+q+2k_F,\sigma_1}^\dagger c_{-,k_2-q-2k_F,\sigma_2}^\dagger c_{+,k_2,\sigma_2} c_{-,k_1,\sigma_1} \\
& + \frac{1}{L} \sum_{\{k,q,\sigma\}} \left(g_2 + 2\bar{g}_2 \sin^2 \frac{q}{2} \right) c_{+,k_1+q,\sigma_1}^\dagger c_{-,k_2-q,\sigma_2}^\dagger c_{-,k_2,\sigma_2} c_{+,k_1,\sigma_1} \\
& + \frac{1}{2L} \sum_{\{k,q,\sigma\}} \left(g_3 + 2\bar{g}_3 \sin^2 \frac{q}{2} \right) \left(c_{+,k_1+q+2k_F,\sigma_1}^\dagger c_{+,k_2-q-2k_F+G,\sigma_2}^\dagger c_{-,k_2,\sigma_2} c_{-,k_1,\sigma_1} + \text{H.c.} \right) \quad (2) \\
& + \frac{1}{2L} \sum_{\{k,q,\sigma\}} \left(g_4 + 2\bar{g}_4 \sin^2 \frac{q}{2} \right) c_{+,k_1+q,\sigma_1}^\dagger c_{+,k_2-q,\sigma_2}^\dagger c_{+,k_2,\sigma_2} c_{+,k_1,\sigma_1} \\
& + \frac{1}{2L} \sum_{\{k,q,\sigma\}} \left(g_4 + 2\bar{g}_4 \sin^2 \frac{q}{2} \right) c_{-,k_1+q,\sigma_1}^\dagger c_{-,k_2-q,\sigma_2}^\dagger c_{-,k_2,\sigma_2} c_{-,k_1,\sigma_1},
\end{aligned}$$

where $\epsilon_k = -2t \cos k$ is the tight-binding spectrum, and $v = 2t$ is the bare Fermi velocity; the Fermi points are $k_F = \pm \frac{\pi}{2}$ at half-filling (here the lattice constant has been set to unity, and $\hbar = 1 = k_B$). By analogy with the ‘g-ology’ description of interactions, we have proceeded to the splitting of the U and V interaction terms into couplings for right ($p = +$, $k > 0$) and left ($p = -$, $k < 0$) moving electrons. We thus obtain momentum independent (local) as well as momentum dependent (non local) couplings, denoted in (2) by $g_{i=1\dots 4}$ and $\bar{g}_{1\dots 4}$, respectively. The pairs of couplings for backscattering (g_1, \bar{g}_1) and Umklapp (g_3, \bar{g}_3) have the bare amplitudes $g_{1,3} = U - 2V, \bar{g}_{1,3} = 2V$, whereas $g_{2,4} = U + 2V$ and $\bar{g}_{2,4} = -2V$ stand for the amplitudes for the forward scattering between opposite (g_2, \bar{g}_2) and parallel (g_4, \bar{g}_4) k electrons.

The information about the lattice in (2) is present by the use of the tight binding spectrum ϵ_k for $k \in [-\pi, \pi]$ in the Brillouin zone and in the momentum dependent couplings $\bar{g}_i \sin^2 q/2$. In the continuum limit, the latter amplitudes vanish when evaluated at zero momentum transfer, while the spectrum $\epsilon_k \rightarrow \epsilon_p(k) \approx v(pk - k_F)$ is taken as linear around each Fermi points. One thus recovers the standard electron gas formulation of the extended Hubbard model¹⁻⁴.

B. The renormalization group transformation

We write the partition function $Z = \text{Tr} e^{-\beta H}$ as a functional integral

$$Z = \int \int \mathcal{D}\psi^* \mathcal{D}\psi e^{S[\psi^*, \psi]}, \quad (3)$$

over anticommuting Grassmann fields $\psi^{(*)}$. The action $S[\psi^*, \psi] = S_0[\psi^*, \psi] + S_I[\psi^*, \psi]$ consists of a free and an interacting parts. In the Fourier-Matsubara space, the former part $S_0[\psi^*, \psi]$ reads

$$S_0[\psi^*, \psi] = \sum_{p, \bar{k}, \sigma} [G_p^0(\bar{k})]^{-1} \psi_{p,\sigma}^*(\bar{k}) \psi_{p,\sigma}(\bar{k}), \quad (4)$$

where

$$G_p^0(\bar{k}) = [i\omega_n - \epsilon_k]^{-1}, \quad (5)$$

is the free electron propagator. Here $\bar{k} = (k, \omega_n)$ and $\omega_n = (2n + 1)\pi T$ is the fermion Matsubara frequency. The interacting part is given by

$$\begin{aligned}
S_I[\psi^*, \psi] = & -\frac{T}{L} \sum_{\{\bar{k}, \bar{q}, \sigma\}} \left(g_1 + 2\bar{g}_1 \sin^2 \frac{q}{2} \right) \psi_{+, \sigma_1}^* (\bar{k}_1 + \bar{q}_0 + \bar{q}) \psi_{-, \sigma_2}^* (\bar{k}_2 - \bar{q}_0 - \bar{q}) \psi_{+, \sigma_2} (\bar{k}_2) \psi_{-, \sigma_1} (\bar{k}_1) \\
& -\frac{T}{L} \sum_{\{\bar{k}, \bar{q}, \sigma\}} \left(g_2 + 2\bar{g}_2 \sin^2 \frac{q}{2} \right) \psi_{+, \sigma_1}^* (\bar{k}_1 + \bar{q}) \psi_{-, \sigma_2}^* (\bar{k}_2 - \bar{q}) \psi_{-, \sigma_2} (\bar{k}_2) \psi_{+, \sigma_1} (\bar{k}_1) \\
& -\frac{T}{2L} \sum_{\{\bar{k}, \bar{q}, \sigma\}} \left(g_3 + 2\bar{g}_3 \sin^2 \frac{q}{2} \right) (\psi_{+, \sigma_1}^* (\bar{k}_1 + \bar{q}_0 + \bar{q}) \psi_{+, \sigma_2}^* (\bar{k}_2 - \bar{q}_0 - \bar{q} + \bar{G}) \psi_{-, \sigma_2} (\bar{k}_2) \psi_{-, \sigma_1} (\bar{k}_1) + \text{c.c.}) \\
& -\frac{T}{2L} \sum_{\{\bar{k}, \bar{q}, \sigma\}} \left(g_4 + 2\bar{g}_4 \sin^2 \frac{q}{2} \right) \psi_{+, \sigma_1}^* (\bar{k}_1 + \bar{q}) \psi_{+, \sigma_2}^* (\bar{k}_2 - \bar{q}) \psi_{+, \sigma_2} (\bar{k}_2) \psi_{+, \sigma_1} (\bar{k}_1) \\
& -\frac{T}{2L} \sum_{\{\bar{k}, \bar{q}, \sigma\}} \left(g_4 + 2\bar{g}_4 \sin^2 \frac{q}{2} \right) \psi_{-, \sigma_1}^* (\bar{k}_1 + \bar{q}) \psi_{-, \sigma_2}^* (\bar{k}_2 - \bar{q}) \psi_{-, \sigma_2} (\bar{k}_2) \psi_{-, \sigma_1} (\bar{k}_1),
\end{aligned} \tag{6}$$

where $\bar{q} = (q, \omega_m)$, $\omega_m = 2\pi mT$, $\bar{q}_0 = (2k_F, 0)$; here $\bar{G} = (4k_F, 0)$ is a reciprocal lattice vector that enters in the definition of Umklapp scattering at half-filling.

The momentum shell K-W RG transformation is based upon the recursive application of the two following steps for the partition function. In the first step, a partial trace of Z over outer shell electronic degrees of freedom denoted by $\bar{\psi}_{p, \sigma}(k, \omega_n)$, is carried out at all ω_n and spin σ . The outer momentum shell is defined by the intervals of momentum

$$\begin{aligned}
k \in [0, k_F - k_0/s[\cup]k_F + k_0/s, \pi], \quad p = + \\
\in]-k_F + k_0/s, 0] \cup [-\pi, -k_F - k_0/s[, \quad p = -.
\end{aligned} \tag{7}$$

above and below the Fermi level for each branch p . Here $k_0 = \pi/2$ is a cutoff wave vector defined with respect to the Fermi points $(\pm k_F \pm k_0 = \pm\pi)$, and $s = e^{d\ell} > 1$ is the momentum scaling factor for $d\ell \ll 1$. The second step consists in the rescaling of the momentum distance from the Fermi points we call δk ; this gives $k' = \pm k_F + s\delta k$, which restores the initial cutoff $k_0 = \pi/2$ of the lattice model.

The two recursive steps of the RG transformation can be expressed as

$$\begin{aligned}
Z = & \left[\int \int_{<} \mathcal{D}\psi^* \mathcal{D}\psi e^{S[\psi^*, \psi]_\ell} \int \int \mathcal{D}\bar{\psi}^* \mathcal{D}\bar{\psi} e^{S_0[\bar{\psi}^*, \bar{\psi}]} \right. \\
& \left. \times e^{\sum_{i=1}^4 S_{I,i}[\bar{\psi}^*, \bar{\psi}, \psi^*, \psi]} \right]_{\psi \rightarrow \zeta_s^{\frac{1}{2}} \psi'} \\
\propto & \left[\int \int_{<} \mathcal{D}\psi^* \mathcal{D}\psi e^{S[\psi^*, \psi]_\ell + \langle S_{I,2} \rangle_{\bar{0},c} + \frac{1}{2} \langle (S_{I,2})^2 \rangle_{\bar{0},c} + \dots} \right]_{\psi \rightarrow \zeta_s^{\frac{1}{2}} \psi'},
\end{aligned} \tag{8}$$

where $S_{I,i}$ is the interacting part of the action with $i = 1, \dots, 4$, $\bar{\psi}$ fields in the outer momentum shell. The outer shell statistical averages $\langle \dots \rangle_{\bar{0},c}$ over the variables $\bar{\psi}^{(*)}$ are performed with respect to $S_0[\bar{\psi}^*, \bar{\psi}]$. These averages correspond to the sum of all connected diagrams with

even number of external fields ψ^*, ψ pertaining to the inner momentum shell ($<$) degrees of freedom, which are kept fixed in the partial trace operation. At the one-loop level the partial trace and rescaling lead to the recursion relations

$$\left[S_0[\psi^*, \psi]_{\ell+d\ell} = S_0[\psi^*, \psi]_\ell + \langle S_{I,2} \rangle_{\bar{0},c} + \dots \right]_{\psi \rightarrow \zeta_s^{\frac{1}{2}} \psi'}, \tag{9}$$

$$\left[S_I[\psi^*, \psi]_{\ell+d\ell} = S_I[\psi^*, \psi]_\ell + \frac{1}{2} \langle S_{I,2}^2 \rangle_{\bar{0},c} + \dots \right]_{\psi \rightarrow \zeta_s^{\frac{1}{2}} \psi'}, \tag{10}$$

for the free and interacting parts of the action.

Following the momentum rescaling, the inner shell fields ψ are rescaled by the factor $\zeta_s^{1/2}$, which can be derived from a dimensional analysis of the parameters that define the bare action S_0 . Thus assuming that the rescaling of the tight-binding spectrum is of the form $\epsilon'_{k'} \equiv \zeta_s \epsilon_k$, by taking $k' = \pm k_F + s\delta k$, one gets in the limit $d\ell \rightarrow 0$

$$\zeta_s \rightarrow \zeta_s(\delta k) = s^{\delta k \cot \delta k}, \tag{11}$$

which can be expressed in the form s^y compatible with an iterative transformation in renormalization group. At variance with the usual case, however, the scaling dimension y is here k dependent. Thus at either the edge or the bottom of the band where the group velocity vanishes, $\zeta_s(\pm k_0) \rightarrow s^0$ and ϵ_k is dimensionless. It is only when the Fermi points is approached in the limit $\delta k \rightarrow 0$, that $\zeta_s(\delta k) \rightarrow s^1$ and the result of the continuum limit for a linear spectrum is recovered¹³. This also indicates that repetition of rescaling turns down the curvature of the band, which continuously evolves toward a linear shape. Since ω_n or the temperature T enters on the same footing as ϵ_k in the inverse propagator $[G^0]^{-1}$, the temperature then transforms according to $T' = \zeta_s(\delta k)T$. Now referring to the form of S_0 in (4), this yields the transformation assumed above for the field, namely $\psi^{(*)'} = \zeta_s^{-1/2}(\delta k) \psi^{(*)}$.

When applied to the interacting part S_I of the the action, the above relations for the field and temperature, combined to the shrinking of the number sites $L' = L/s$ under rescaling, will impose the following k -dependent transformations of interactions

$$g'_i = (g_i + \mathcal{O}(g^2)) s^{-1+\delta k \cot \delta k}, \quad (12)$$

$$\bar{g}'_i = (\bar{g}_i + \mathcal{O}(g\bar{g})) s^{-1-\delta k \csc \delta k}. \quad (13)$$

It ensues that for $\delta k \rightarrow \pm k_0$, we have $g'_i \rightarrow g_i s^{-1}$, and the local couplings are then irrelevant instead of being marginal variables near the bottom or the edge of the band. At the approach of the Fermi level, when $\delta k \rightarrow 0$, we have $g'_i = g_i$ and the dimensionless or marginal character of the local interactions of the electron gas model is retrieved^{2,13}. In the same way, the non local terms transform according to $\bar{g}'_i = \bar{g}_i s^{-1-\pi/2}$ at the boundaries or the bottom of the band and are therefore strongly irrelevant. In the limit $\delta k \rightarrow 0$ near the Fermi points, $\bar{g}'_i = \bar{g}_i s^{-2}$, which corresponds to the usual negative bare scaling dimension of nearest-neighbor couplings of the continuum theory^{4,16}.

C. The Fermi velocity and coupling constant flow equations

We now proceed to the partial trace operation that defines the first step of the renormalization group transformation (8). At the one-loop level, this amounts to evaluate the outer shell statistical averages $\langle S_{I,2} \rangle_{\bar{0},c}$ and $\langle S_{I,2}^2 \rangle_{\bar{0},c}$ of the recursion relations (9) and (10). The former contribution $\langle S_{I,2} \rangle_{\bar{0},c}$ is composed of Hartree and Fock self-energy corrections. In these, enter k independent or constant terms that correct the chemical potential, a quantity that can be simply redefined to keep the filling of the band constant. These terms can be safely ignored. The presence of non local interactions give rise to momentum dependent Fock terms, which at the step ℓ of the iterative RG procedure read

$$\begin{aligned} \langle S_{I,2} \rangle_{\bar{0},c} &= \frac{T(\ell)}{L(\ell)} \sum_{\bar{k}} \sum_{\bar{k}'} [\bar{g}_1(\ell) G_{-p}^0(\bar{k}') - \bar{g}_4(\ell) G_p^0(\bar{k}')] \\ &\quad \times \cos(k_F + \delta k) \psi_p^*(\bar{k}) \psi_p(\bar{k}), \end{aligned} \quad (14)$$

where the slashed summation contains an integration over k' in the outer momentum shell interval (7) at a given p . The Fock terms contribute to the renormalization of the spectrum, that is the Fermi velocity. Carrying the \bar{k}' summation, one gets the flow equation for the velocity,

$$d_\ell \ln v(\ell) = \frac{\pi}{4} (\bar{g}_4(\ell) - \bar{g}_1(\ell)) \tanh[v(\ell) \sin \delta k_\ell / 2T], \quad (15)$$

where $\delta k_\ell = k_0 e^{-\ell}$ and the couplings $\bar{g} \equiv \bar{g}/\pi v(\ell)$ are henceforth taken as normalized by the scale dependent Fermi velocity $v(\ell)$.

The recursion relations (12) for the local normalized couplings $\bar{g}(\equiv g/\pi v(\ell))$ are obtained from the outer shell contractions $\langle S_{I,2}^2 \rangle_{\bar{0},c}$ in the logarithmically singular Cooper (electron-electron) and Peierls ($2k_F$ electron-hole) channels. Their insertion in (12), leads after rescaling to the recursion relations

$$\bar{g}'_1 = [\bar{g}_1 + (-\bar{g}_1^2 + \bar{g}_3 \bar{g}_3) I_P + \bar{g}_1(\bar{g}_2 + \bar{g}_2) I_C] s^{-f_g} \quad (16)$$

$$\bar{g}'_2 = [\bar{g}_2 + (\bar{g}_1 + \bar{g}_1)^2 I_C + (\bar{g}_3 + \bar{g}_3)^2 I_P] s^{-f_g} \quad (17)$$

$$\begin{aligned} \bar{g}'_3 &= [\bar{g}_3 + (\bar{g}_2 + \bar{g}_2)(2\bar{g}_3 + \bar{g}_3) I_P \\ &\quad - (\bar{g}_1 + \bar{g}_1)(\bar{g}_3 - \bar{g}_3) I_P] s^{-f_g} \end{aligned} \quad (18)$$

$$\bar{g}'_4 = \bar{g}_4 s^{-f_g}, \quad (19)$$

where $f_g = 1 - \delta k_\ell \cot \delta k_\ell + d_\ell \ln v(\ell)$, which contains the rescaling exponent of (12), and the correction due to the normalization from the scale dependent Fermi velocity. We note that the one-loop level, there is no logarithmic correction to the forward scattering amplitude g_4 . The outer shell Cooper and Peierls loops evaluated at zero external variables are respectively given by

$$\begin{aligned} I_C &= -2\pi v(\ell) \frac{T(\ell)}{L(\ell)} \sum_{k>0} \sum_{\omega_n} G_+^0(\bar{k} + \bar{q}_C) G_-^0(-\bar{k}) \\ &= -\pi v(\ell) \frac{1}{L(\ell)} \sum_{k>0} \frac{\tanh[\epsilon(k)/2T(\ell)]}{\epsilon(k)} \\ &= -\frac{\pi}{2} \tanh[\epsilon(\ell)/2T] d\ell \end{aligned} \quad (20)$$

at $\bar{q}_C = 0$, where $\epsilon(\ell) = v(\ell) \sin \delta k_\ell$ and

$$\begin{aligned} I_P(\ell) &= -2\pi v(\ell) \frac{T(\ell)}{L(\ell)} \sum_k \sum_{\omega_n} G_+^0(\bar{k} + \bar{q}_P) G_-^0(k) \\ &= -I_C \end{aligned} \quad (21)$$

at $\bar{q}_P = (2k_F, 0)$. It is worth stressing that neglecting the dependence of $I_{P,C}$ on external variables does not generate new momentum dependent interactions whose number is kept fixed along the RG flow.

The flow equations for the local interactions then become

$$d_\ell \bar{g}_1 = -f_g \bar{g}_1 + f_1 [-\bar{g}_1^2 - \bar{g}_1(\bar{g}_2 + \bar{g}_2) + \bar{g}_3 \bar{g}_3], \quad (22)$$

$$d_\ell \bar{g}_2 = -f_g \bar{g}_2 + \frac{1}{2} f_1 [(\bar{g}_3 + \bar{g}_3)^2 - (\bar{g}_1 + \bar{g}_1)^2], \quad (23)$$

$$\begin{aligned} d_\ell \bar{g}_3 &= -f_g \bar{g}_3 + f_1 [(\bar{g}_2 + \bar{g}_2)(2\bar{g}_3 + \bar{g}_3) \\ &\quad - (\bar{g}_1 + \bar{g}_1)(\bar{g}_3 - \bar{g}_3)], \end{aligned} \quad (24)$$

$$d_\ell \bar{g}_4 = -f_g \bar{g}_4, \quad (25)$$

where $f_1 = \frac{\pi}{2} \tanh[\epsilon(\ell)/2T]$. These equations differs from the usual scaling equations of the 1D-EG model in two respects. First, the rescaling for a tight-binding spectrum and velocity renormalization introduce linear terms; second, there are additional corrections coming to the coupling to momentum dependent interactions. These latter corrections are by far the most likely to influence the flow

of local couplings if not the nature of the ground state as we will see.

As for the non local irrelevant interactions, the corrections due to loop contractions are small and will be neglected in weak coupling. From the rescaling transformation (13) and the normalization of the couplings by $\pi v(\ell)$, we get

$$d_\ell \tilde{g}_i = - (1 + \delta k_\ell \csc \delta k_\ell + d_\ell \ln v(\ell)) \tilde{g}_i \quad (26)$$

for $i = 1, \dots, 4$. In the zero temperature limit, the solution of Eqs. (15) and (26) yields the following expressions

$$v(\ell) = v \left(1 - \frac{V}{\pi t} \ln[2 \cos^2(\delta k_\ell/2)] \right), \quad (27)$$

for the Fermi velocity and

$$\bar{g}_i(\ell) = \bar{g}_i \frac{v}{v(\ell)} e^{-\ell} \tan(\delta k_\ell/2), \quad (28)$$

for the non-local couplings. The Fermi velocity is thus renormalized downward due to the presence of the V term; it reaches the value $v^* = v(1 - \frac{V}{\pi t} \ln 2)$ in the limit of large ℓ .

D. Response Functions

To determine the nature of long-range correlations in the ground state, we consider the most singular response functions or susceptibilities, which are denoted χ_μ . These latter are obtained by adding to the $\ell = 0$ action an additional term S_h^{13} , which consists of source fields h_μ linearly coupled to the composite fields O_μ^* ,

$$S_h[\psi^*, \psi] = \sum_{\mu, \bar{q}} [h_\mu(\bar{q}) z_\mu O_\mu^*(\bar{q}) + \text{c.c.}], \quad (29)$$

where z_μ is a pair vertex renormalization factor ($z_\mu = 1$ at $\ell = 0$). In what follows we shall examine the site spin density-wave ($\mu = \text{SDW}$), bond spin density-wave ($\mu = \text{BSDW}$), site charge density-wave ($\mu = \text{CDW}$) and the bond order-wave ($\mu = \text{BOW}$) susceptibilities of the Peierls channel; the singlet (SS) and triplet (TS) superconducting susceptibilities of the Cooper channel. These are defined with the aid of the following expressions for the composite pair fields,

$$O_{\text{SDW/BSDW}}(\bar{q}) = \frac{1}{2} (O_{x,y,z}^*(-\bar{q}) \pm O_{x,y,z}(\bar{q})) \quad (30)$$

and

$$O_{\text{CDW/BOW}}(\bar{q}) = \frac{1}{2} (O_0^*(-\bar{q}) \pm O_0(\bar{q})) \quad (31)$$

in the Peierls channel, where

$$O_\mu(\bar{q}) = \sqrt{\frac{T}{L}} \sum_{\bar{k}} \psi(\bar{k} - \bar{q})_{-, \alpha}^* \sigma_\mu^{\alpha\beta} \psi_{+, \beta}(\bar{k}),$$

and

$$O_{\text{SS}}(\bar{q}) = \sqrt{\frac{T}{L}} \sum_{\bar{k}} \alpha \psi(-\bar{k} + \bar{q})_{-, -\alpha}^* \psi_{+, \alpha}(\bar{k}), \quad (32)$$

$$O_{\text{TS}_\mu}(\bar{q}) = \sqrt{\frac{T}{L}} \sum_{\bar{k}} \alpha \psi(-\bar{k} + \bar{q})_{-, -\alpha}^* \sigma_\mu^{\alpha\beta} \psi_{+, \beta}(\bar{k}) \quad (33)$$

in the Cooper channel. Here $\sigma_{\mu=x,y,z}(\sigma_0)$ are the Pauli (identity) matrices.

The renormalization group transformation (8) at the one-loop level, will modify S_h according to

$$S_h[O^*, O]_{\ell+d\ell} = \left[S_h[O^*, O]_\ell + \langle S_h S_{I,2} \rangle_{\bar{0},c} + \dots \right]_{O^{(*)} \rightarrow s^0 O'^{(*)}} + \frac{1}{2} \langle S_h^2 \rangle_{\bar{0},c} + \dots, \quad (34)$$

where the pair fields, having zero canonical dimension, remain unchanged under rescaling. The last term is a constant $\propto d\ell z_\mu^2 h_\mu^* h_\mu$ that adds at each iteration and yields the expression of the susceptibility

$$\pi v \chi_\mu(\bar{q}_\mu^0) = \frac{\pi}{2} \int_\ell \frac{v}{v(\ell)} z_\mu^2 \tanh[\epsilon(\ell)/2T] d\ell, \quad (35)$$

which is defined positive and evaluated in the static limit at $\bar{q}_\mu^0 = (2k_F, 0)$ and $(0, 0)$ for the Peierls and Cooper channels, respectively. From the one-loop outer shell corrections to the linear coupling, which read

$$\langle S_h S_{I,2} \rangle_{\bar{0},c} = \frac{\pi}{2} \tanh[\epsilon(\ell)/2T] d\ell \sum_{\mu, \bar{q}} [h_\mu(\bar{q}) \tilde{g}_\mu z_\mu O_\mu^*(\bar{q}) + \text{c.c.}],$$

one gets the one-loop equation for the pair vertex part z_μ at \bar{q}_μ^0 ,

$$d_\ell \ln z_\mu = \tilde{g}_\mu \frac{\pi}{2} \tanh[\epsilon(\ell)/2T]. \quad (36)$$

For the density-wave type susceptibilities, the normalized couplings \tilde{g}_μ are given by the combinations

$$\tilde{g}_{\text{CDW/BOW}} = -2\tilde{g}_1 + \tilde{g}_2 + \tilde{g}_2 \mp \tilde{g}_3 \pm \tilde{g}_3, \quad (37)$$

$$\tilde{g}_{\text{SDW/BSDW}} = \tilde{g}_2 \pm \tilde{g}_3 + \tilde{g}_2 \pm \tilde{g}_3. \quad (38)$$

The corresponding expressions for the superconducting susceptibilities are

$$\tilde{g}_{\text{SS/TS}} = \mp \tilde{g}_1 - \tilde{g}_2 \mp \tilde{g}_1 - \tilde{g}_2. \quad (39)$$

A positive value for \tilde{g}_μ at $\ell \rightarrow \infty$ signals a singularity in z_μ and then in χ_μ in that limit.

III. RESULTS

The solution of the flow equations for the pair vertices (36) and the couplings (22-26) in the $T \rightarrow 0$ limit

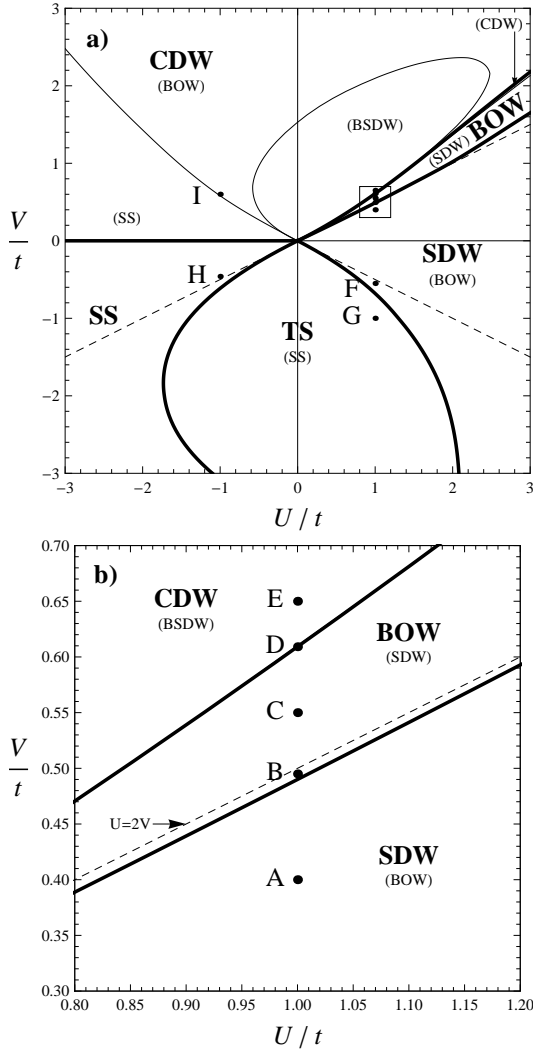


FIG. 1: a) The phase diagram of the 1D extended Hubbard model. The bold (thin) lines refer to the boundaries between the primary (secondary) phases indicated in bold (regular) characters. The dashed lines correspond to the boundaries of the phase diagram of the electron gas model in the continuum limit; b) zoom in the neighborhood of the $U = 2V$ (dashed) line in the repulsive sector.

leads to the determination of the most singular susceptibilities. These in turn serve to the determination of the dominant and subdominant phases of the model in the ground state. This is summarized in the one-loop phase diagram of Fig. 1, as a function of weak U and V . The results are compared with those obtained in the continuum limit^{1,4}.

A. Repulsive U

We commence by looking at the first quadrant of the phase diagram, in the region surrounding the $U = 2V > 0$ line. At the point A below the separatrix in Fig. 1-b,

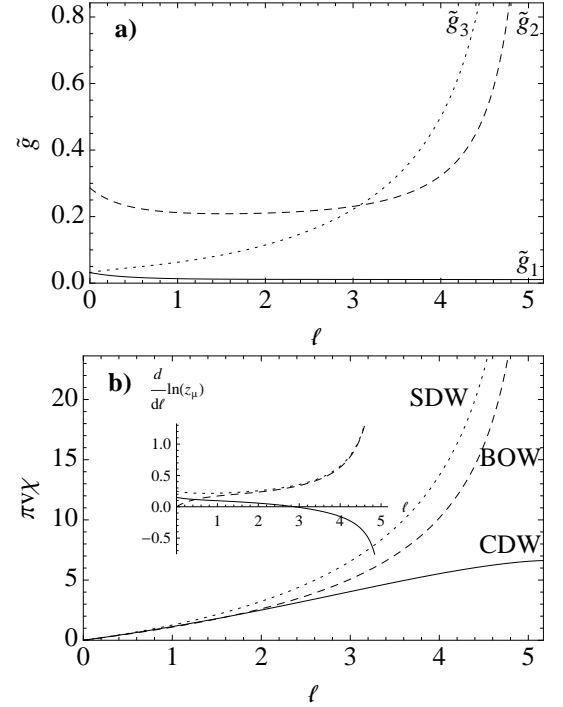


FIG. 2: a) Flow of the coupling constants $\tilde{g}_{1,2,3}$ at the point A (1, 0.4) of the phase diagram in Fig. 1. b) The density-wave susceptibilities vs ℓ ; inset: the flow of the pair vertices $d_\ell \ln z_\mu$ for $\mu = \text{SDW}, \text{BOW}$ and SDW .

where $U > 2V$, the \tilde{g}_2 and \tilde{g}_3 couplings scale to strong repulsive values and become singular at a finite ℓ_ρ , a singularity at one-loop level that is indicative of a (Mott) gap in the charge sector compatible with the initial conditions satisfying the inequality $\tilde{g}_1 - 2\tilde{g}_2 < \tilde{g}_3$. The repulsive \tilde{g}_1 coupling is marginally irrelevant and attributed to gapless spin degrees of freedom. The SDW response then develops a singularity similar to the one of BOW at large $\ell \sim \ell_\rho$, as shown by the behavior of z_{SDW} and z_{BOW} in the inset of Fig. 2-b. From the same Figure, however, the amplitude of the SDW susceptibility is larger, and SDW (BOW) is then taken as the dominant (subdominant) phase in the ground state. These one-loop results indicate that in this region irrelevant non local couplings introduce no qualitative changes with respect to known results of the continuum theory^{1,2,17}.

If we now move up to the point B in the phase diagram of Fig. 1-b, close but below the $U = 2V$ line, a qualitative change with respect to the results of the continuum limit emerges. While \tilde{g}_2 and \tilde{g}_3 still scale to strong repulsive coupling, signaling the formation of a charge gap at a finite ℓ_ρ (Fig. 3-a), the backscattering amplitude \tilde{g}_1 no longer scales toward zero, but extends across the $\tilde{g}_1 = 0$ line to then level off at a small non universal negative value (inset of Fig. 3-a). According to the expressions in (37), this change of sign of \tilde{g}_1 yields $\tilde{g}_{\text{BOW}} > \tilde{g}_{\text{SDW}}$, indicating that the strongest singularity now occurs for the BOW response (inset of Fig. 3-b). The BOW phase

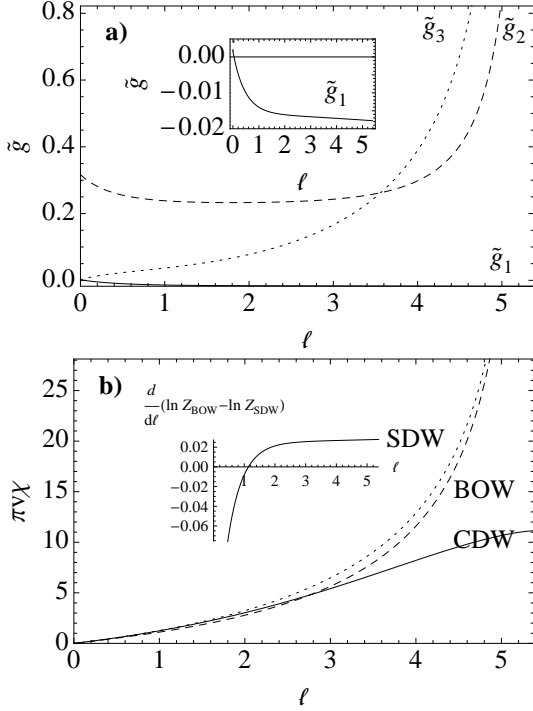


FIG. 3: a) Flow of the coupling constants $\tilde{g}_{1,2,3}$ at point B : (1, 0.495) of the phase diagram in Fig. 1. b) The density-wave susceptibilities *vs* ℓ ; inset: the difference between the BOW and SDW flows of the pair vertices showing the dominance of the BOW phase.

then becomes the dominant phase, whereas SDW closely follows as the secondary phase. The change of sign of \tilde{g}_1 takes its origin in the presence of non local couplings in the flow equations (22-24). Although irrelevant, these interactions push the renormalization of \tilde{g}_1 (\tilde{g}_3) downward (upward) through their coupling to local variables.

The dominance of the BOW phase becomes more pronounced as one moves up across the line $U = 2V$ (point C of Fig. 1-b). In this region, the initial local couplings \tilde{g}_1 and \tilde{g}_3 are negative, but the latter interaction is still pushed to strong repulsive sector by non-local couplings (Fig. 4-a). The BOW susceptibility then develops the strongest singularity with the largest amplitude (Fig. 4-b). These features of the flow and the predominance of BOW order keep on up the BOW-CDW boundary passing just below point D in Fig. 1-b. At that point, strong attractive coupling in \tilde{g}_1 and \tilde{g}_2 is occurring while \tilde{g}_3 remains small and attractive (Fig. 5-a), implying the formation of a gap in the spin sector instead of the charge. In these conditions, we have $\tilde{g}_{\text{CDW}} > \tilde{g}_{\text{BOW}}$, which marks the onset of a dominant CDW phase. The BOW order is subdominant and SDW correlations are non longer singular and are strongly reduced by the presence of a spin gap. It is worth noting that the emergence of a spin gap regime on the BOW-CDW frontier is compatible with the results of quantum Monte Carlo simulations⁷, which find the onset of a Luther-Emery liquid with a spin gap at

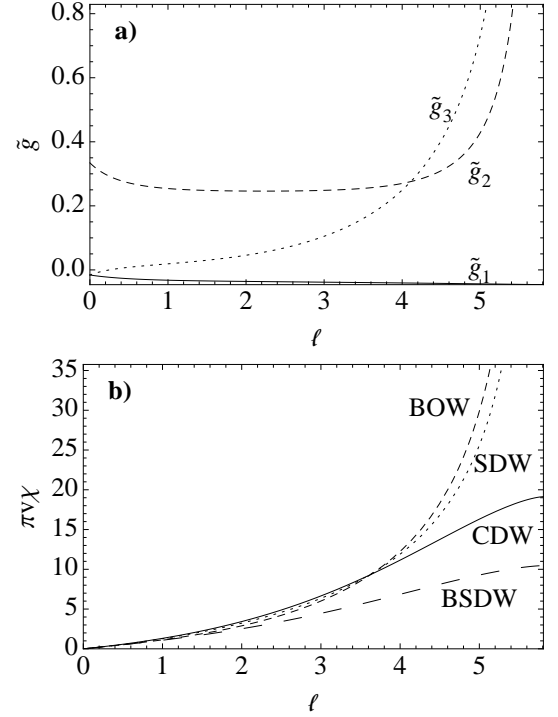


FIG. 4: a) Flow of the $\tilde{g}_{1,2,3}$ couplings at C (1, 0.55) in the phase diagram of Fig. 1. b) The susceptibilities *vs* ℓ ;

the boundary. The same analysis carried out as a function of U allows for the delimitation of a small but finite fan-shape region of the weak coupling phase diagram of Fig. 1 where the BOW order intervenes as the ground state around the $U = 2V$ line. This well known result of numerical calculations⁵⁻⁷ and functional RG¹² contrasts with the direct SDW to CDW transition predicted for the 1D-EG model¹.

We proceed on the analysis of the repulsive U region by looking at the point E, that is above the intermediate BOW region. In this domain, \tilde{g}_2 and \tilde{g}_3 scale to strong repulsive and attractive couplings, respectively, while \tilde{g}_1 is non universal and weakly attractive (Fig. 6-a), contrary to what is found for the electron gas model^{1,2,17}. The CDW singularity is stronger and accompanied by a weaker singularity in the BSDW response (Fig. 6-b). The BSDW replaces BOW as the subdominant phase over a finite domain of the phase diagram at $V > 0$ (Fig. 1-a).

We turn to the point F located in the $V < 0$ region below, but near the $U = -2V$ line, where qualitative changes with respect to the continuum limit are also found. In the framework of the 1D-EG model, the region below the $U = -2V$ line is characterized by the conditions $\tilde{g}_1 > 0$ and $\tilde{g}_1 - 2\tilde{g}_2 > \tilde{g}_3$, respectively for gapless spin and charge degrees of freedom with dominant TS and subdominant SS phases^{1,2}. In the presence of non local couplings, however, while \tilde{g}_1 is marginally irrelevant, both \tilde{g}_2 and \tilde{g}_3 scale to strong repulsive coupling signaling that the charge degrees of freedom are still gapped (Fig. 7-a). Therefore the SDW phase re-

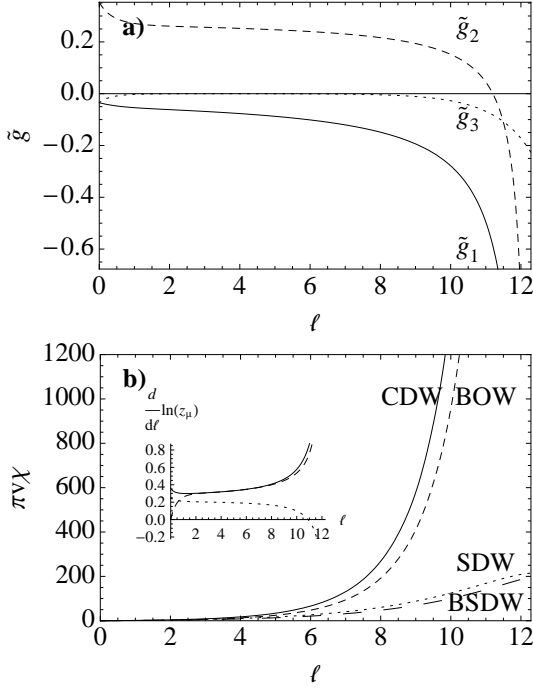


FIG. 5: a) Flow of the $\tilde{g}_{1,2,3}$ couplings at D (1, 0.609) in the phase diagram of Fig. 1. b) The susceptibilities *vs* ℓ ; inset: the flow of the pair vertices $d_\ell \ln z_\mu$ for $\mu = \text{CDW, BOW, and SDW}$

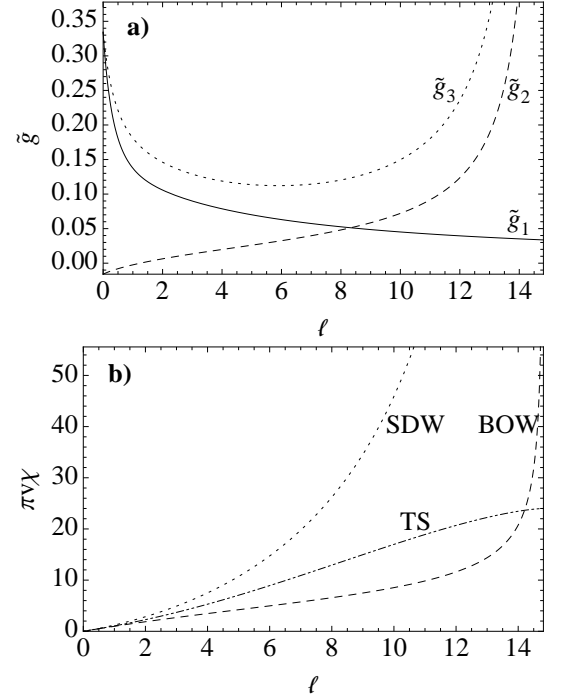


FIG. 7: a) Flow of the $\tilde{g}_{1,2,3}$ couplings at F (1, -0.55) in the phase diagram of Fig. 1. b) The susceptibilities *vs* ℓ .

mains dominant contrary to the 1D-EG prediction of a gapless TS phase^{1,2,17} (Fig. 7-b); the SDW incursion below the $U = -2V$ line expands in size as U increases as shown in Fig. 1-a. It is worth mentioning that the resulting inward bending of the TS-SDW boundary line which becomes more pronounced with increasing U is consistent with the numerical results of Nakamura⁶.

Finally, as one moves sufficiently downward along the V axis, one reaches a region where \tilde{g}_1 and \tilde{g}_3 behave the way marginally irrelevant variables do (Fig 8-a), as shown for instance at the point G of the phase diagram of Fig. 1-a. One then essentially recovers the behavior of the 1D-EG model with a dominant (subdominant) power law singularity $\chi_{\text{TS(SS)}} \propto \exp(\gamma_{\text{TS(SS)}}\ell)$ for TS (SS) response at large ℓ (Fig 8-b) with $\gamma_{\text{TS}} \gtrsim \gamma_{\text{SS}} > 0$.

B. Attractive U

We now consider the region of negative U near the $U = 2V$ line. In this region, we encounter an alteration of the 1D-EG phase diagram boundary that is similar to the one discussed in the last paragraph at $U = -2V > 0$. At H in Fig. 1-b, a portion of the phase diagram with dominant (subdominant) TS (SS) gapless phase is lost, this time to the benefit of a SS phase with a spin gap. Strong attractive coupling in the spin sector is induced by non local couplings that push downward the renormalization of \tilde{g}_1 (Fig. 9-a). As for Umklapp scattering, it stays weakly attractive indicating that the charge sec-

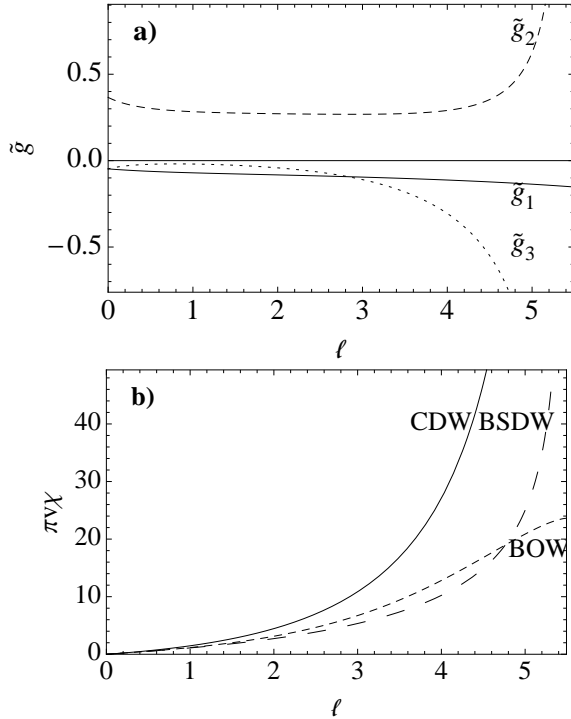


FIG. 6: a) Flow of the $\tilde{g}_{1,2,3}$ couplings at E (1, 0.65) in the phase diagram of Fig. 1. b) The susceptibilities *vs* ℓ .

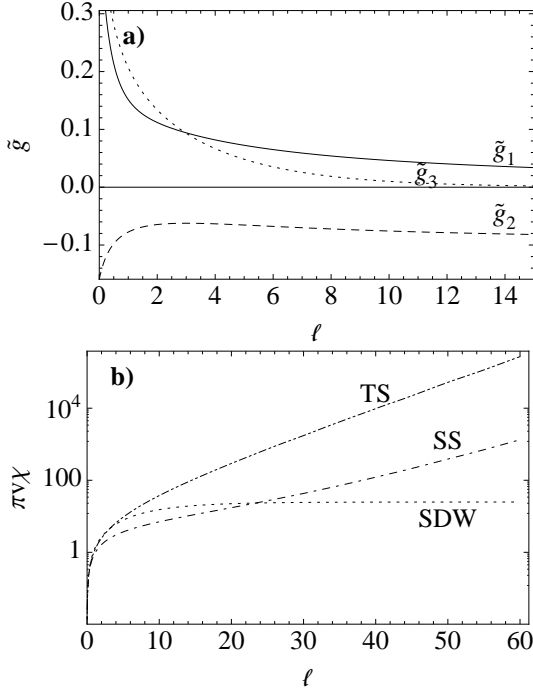


FIG. 8: a) Flow of the $\tilde{g}_{1,2,3}$ couplings at G (1, -1) in the phase diagram of Fig. 1. b) The susceptibilities *vs* ℓ .

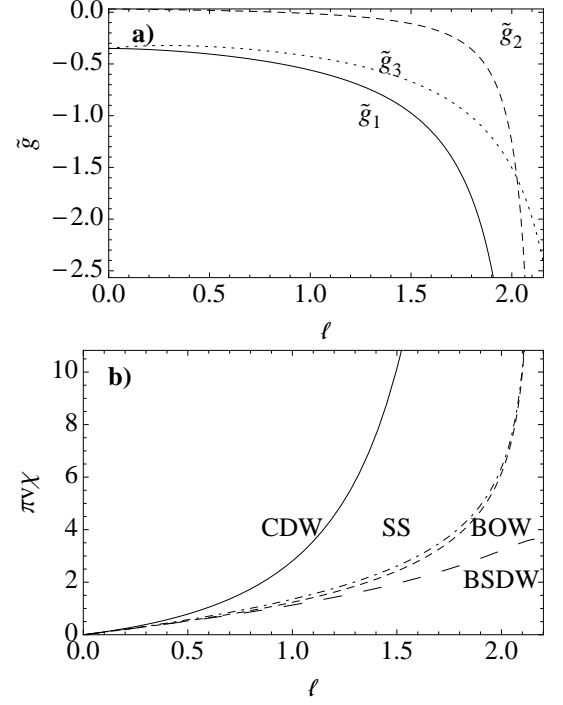


FIG. 10: a) Flow of the $\tilde{g}_{1,2,3}$ couplings at I (-1, 0.6) in the phase diagram of Fig. 1. b) The susceptibilities *vs* ℓ .

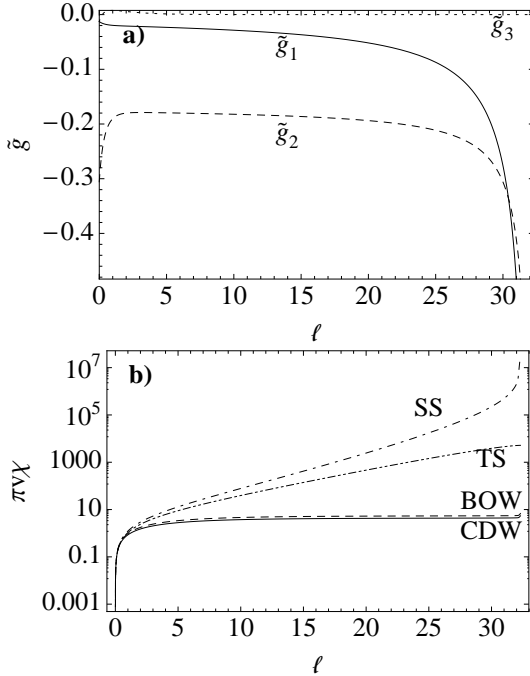


FIG. 9: a) Flow of the $\tilde{g}_{1,2,3}$ couplings at H (-1, -0.46) in the phase diagram of Fig. 1. b) The susceptibilities (logarithmic scale) *vs* ℓ .

tor is gapless. The SS-TS boundary is then distorted inward compared to the straight line 1D-EG prediction, which is in fair agreement with the results of exact diagonalisation by Nakamura.⁶ The SS phase expands from the bent boundary with the TS phase up to the $V = 0$ symmetry line for the transition to CDW (Fig. 1-a). We exemplify the SS region by the point H of the phase diagram (Fig. 1-a), where the \tilde{g}_1 and \tilde{g}_2 scale to strong attractive coupling for the formation of a spin gap at ℓ_σ (Fig. 9-a). The SS response is the only singular response of the system and the whole region has no subdominant phase (Fig. 9-b).

We end the tour of the phase diagram with the second quadrant above the $V = 0$ SS-CDW frontier at the point I. There, the rapid flow to strong attractive coupling for \tilde{g}_1 marks the onset of a spin gap at relatively small ℓ_σ (Fig. 10-a). The strong attraction for \tilde{g}_1 prevails over the Umklapp term, though also marginally relevant. The singularity of the CDW response is thus by far prevalent, being followed by a much weaker BOW susceptibility, whose subdominance is less guaranteed since it occurs in the strong coupling domain where the perturbative RG becomes less reliable.

IV. CONCLUSION

In this work we have proposed a generalization of the momentum shell renormalization group transformation that is applicable to 1D lattice models of interacting

electrons. The approach has been put to the test for the determination of the phase diagram of the extended Hubbard model in weak coupling. The method discloses the influence of a finite number of dangerous irrelevant couplings on the scaling of marginal interaction terms of the model. Modification of scaling gives rise in some regions of the phase diagram to unexpected phases from the standpoint of the theory in the continuum limit. Among the results obtained, let us mention the incursion of BOW order in a finite portion of the repulsive $U \simeq 2V$ sector of the phase diagram, which agrees with previous results of numerical and functional RG methods. The approach is also able to capture the deformation of boundaries between Luttinger liquid and gapped phases in the phase diagram of the model as found previously by exact diag-

onalisation.

These findings are encouraging for applications to other weak coupling 1D or quasi-1D interacting electron models in which lattice details can play an important role in the properties of correlations at long distance.

Acknowledgments

C. B thanks the National Science and Engineering Research Council of Canada (NSERC), the Réseau Québécois des Matériaux de Pointe (RQMP) and the *Quantum materials* program of Canadian Institute of Advanced Research (CIFAR) for financial support.

-
- ¹ V. J. Emery, in *Highly Conducting One-Dimensional Solids*, edited by J. T. Devreese, R. E. Evrard, and V. E. van Doren (Plenum, New York, 1979), p. 247.
 - ² J. Solyom, *Adv. Phys.* **28**, 201 (1979).
 - ³ J. Voit, *Rep. Prog. Phys.* **58**, 977 (1995).
 - ⁴ T. Giamarchi, *Quantum Physics in One Dimension* (Oxford University Press, Oxford, 2004).
 - ⁵ M. Nakamura, *J. Phys. Soc. Jpn.* **68**, 3123 (1999).
 - ⁶ M. Nakamura, *Phys. Rev. B* **61**, 16377 (2000).
 - ⁷ A. W. Sandvik, L. Balents, and D. K. Campbell, *Phys. Rev. Lett.* **92**, 236401 (2004).
 - ⁸ Y. Z. Zhang, *Phys. Rev. Lett.* **92**, 246404 (2004).
 - ⁹ J. Voit, *Phys. Rev. B* **45**, 4027 (1992).
 - ¹⁰ G. I. Japaridze and A. M. Kampf, *Phys. Rev. B* **59**, 12822 (1999).
 - ¹¹ M. Tsuchiizu and A. Furusaki, *Phys. Rev. Lett.* **88**, 056402 (2002).
 - ¹² K.-M. Tam, S.-W. Tsai, and D. K. Campbell, *Phys. Rev. Lett.* **96**, 036408 (2006).
 - ¹³ C. Bourbonnais and L. G. Caron, *Int. J. Mod. Phys. B* **5**, 1033 (1991).
 - ¹⁴ C. Bourbonnais, B. Guay, and R. Wortis, in *Theoretical methods for strongly correlated electrons*, edited by D. Sénéchal, A. M. Tremblay, and C. Bourbonnais (Springer, Heidelberg, 2003), p. 77, cond-mat/0204163.
 - ¹⁵ A similar renormalization group transformation has been first used in the context the XXZ spin chain by B. Dumoulin, C. Bourbonnais, S. Ravy, J.P. Pouget and C. Coulon, *Phys. Rev. Lett.* **76**, 1360 (1996); B. Dumoulin, Ph. D. Thesis, Université de Sherbrooke (1997), unpublished.
 - ¹⁶ F. D. M. Haldane, *Phys. Rev. B* **25**, 4925 (1982).
 - ¹⁷ M. Kimura, *Prog. Theor. Phys.* **63**, 955 (1975).